Physiologically Based Pharmacokinetic Model for T84.66: A Monoclonal Anti-CEA Antibody

SHWETA R. URVA,[1] VICTOR C. YANG,[2] JOSEPH P. BALTHASAR[1]

[1]Department of Pharmaceutical Sciences, University at Buffalo, The State University of New York, Buffalo, New York 14260

[2]Department of Pharmaceutical Sciences, College of Pharmacy, The University of Michigan, 428 Church Street, Ann Arbor, Michigan 48109-1065

Received 25 November 2008; revised 19 June 2009; accepted 25 July 2009

Published online 22 September 2009 in Wiley InterScience (www.interscience.wiley.com). DOI 10.1002/jps.21918

ABSTRACT: Antibodies directed against tumor associated antigens are being increasingly used for detection and treatment of cancers; however, there is an incomplete understanding of the physiological determinants of antibody pharmacokinetics and tumor distribution. The purpose of this study is to (a) compare the plasma pharmacokinetics of T84.66, a monoclonal anti-CEA antibody directed against tumor associated carcinoembryonic antigen (CEA), in control and CEA expressing LS174T xenograft bearing mice, and (b) to develop a physiologically based pharmacokinetic (PBPK) model capable of integrating the influence of CEA and the IgG salvage receptor, FcRn, on T84.66 disposition. T84.66 pharmacokinetics were studied following i.v. administration (1, 10, 25 mg/kg) in control and xenograft bearing mice. In control mice, no significant differences in clearance were observed across the dose range studied. In mice bearing xenograft tumors, clearance was increased by four- to sevenfold, suggesting the presence of a "target mediated" elimination pathway. T84.66 plasma disposition was characterized with a PBPK model, and the model was applied to successfully predict antibody concentrations in tumor tissue. The PBPK model will be used to assist in the development of antibody-based targeting strategies for CEA-positive tumors. © 2009 Wiley-Liss, Inc. and the American Pharmacists Association J Pharm Sci 99:1582–1600, 2010

Keywords: pharmacokinetics; physiological model; PBPK; T84.66 anti-CEA antibody; tumor associated antigen; carcinoembryonic antigen (CEA); target mediated disposition; mathematical model; preclinical pharmacokinetics

INTRODUCTION

Monoclonal antibodies[1] have been investigated for use as "magic bullets" to target a desired site of action, while minimizing unwanted side effects. The number of antibodies approved in the oncology area has steadily increased over recent years and, at present, nine monoclonal antibodies have been FDA-approved for use in cancer treatment. More than 20 antibodies aimed at different antigen targets are presently in clinical oncology trials.[2]

Immune gamma globulin (IgG) is the most prevalent antibody isotype found in man, with average serum concentrations in the range of 10–12 mg/mL.[3] Virtually all mAb that are in development are IgG antibodies. Compared to other immunoglobulin isotypes, IgG has the longest half-life and lowest fractional catabolic rate.[4] In 1964, Brambell proposed that specific transport proteins were capable of binding to IgG and limiting its elimination. With increasing IgG concentrations, these receptors would get

Correspondence to: Joseph P. Balthasar (Telephone: 716-645-2842 ext 270; Fax: 716-645-3693; E-mail: jb@buffalo.edu)

Journal of Pharmaceutical Sciences, Vol. 99, 1582–1600 (2010)

saturated, and the excess unbound IgG would face catabolism.[5] Further research has led to the isolation and cloning of this transport protein, and it has been named "FcRn" or the Fc-receptor of the neonate.[6,7] Various groups have now demonstrated the role of FcRn as a salvage receptor protecting IgG from elimination.[8–10] FcRn has been shown to be expressed in the vascular endothelial cells of various tissues and plays a key role in maintaining IgG homeostasis. However, in addition to FcRn, interaction of an antibody with its target antigen may be a very important determinant of antibody disposition.[11]

A number of FDA-approved mAb demonstrate "target mediated elimination,"[12] where antibody elimination is mediated by specific binding to targets such as epidermal growth factor receptor (EGFR), CD33, CD11 and Her2.[11,13] Carcinoembryonic antigen (CEA)[14] is one of the most widely studied tumor-associated antigens, and it is known to be expressed at low levels in normal tissues such as epithelial cells of the esophagus, pancreas, uterus and prostrate, mucous stomach cells and ducts of sweat glands.[15–18] CEA levels are increased by several fold in a wide range of adenocarcinomas including breast cancers, colorectal cancers, and other cancers of the gastrointestinal tract. Their differential expression offers a possibility for discrimination between normal tissues and tumor cells, making CEA an extremely attractive target for antibody-directed tumor imaging[19–21] or drug targeting.[22,23] However, the influence of tumor-associated CEA on the plasma pharmacokinetics of anti-CEA antibodies has not been thoroughly investigated.

In this work, we have developed a physiologically based pharmacokinetic (PBPK) model incorporating a target-mediated disposition component to examine the influence of antigen–antibody interaction on antibody pharmacokinetics. The model also incorporates additional, known complexities associated with antibody disposition such as: convective uptake into tissues, FcRn-mediated protection within endosomes of the vascular endothelium, and the influence of endogenous antibody levels on the FcRn-mediated transport of therapeutic antibody. Plasma concentration data were collected from mice bearing tumors expressing CEA and control mice lacking the tumor-associated antigen. The PBPK model was able to capture the plasma data in control mice and in antigen-positive tumor-bearing mice, and the model was shown to predict T84.66 antibody concentrations within tumor tissue.

MATERIALS AND METHODS

Production and Purification of T84.66

Hybridoma cells producing T84.66, a monoclonal anti-CEA antibody, were purchased from the American Type Culture Collection (ATCC # HB-8747, Manassas, VA). T84.66 is known to bind CEA with an equilibrium dissociation constant of 3.8×10^{-11} M.[24] For the purposes of antibody production, cells were grown in 1L spinner flasks containing serum free media (Hybridoma SFM, Invitrogen, NY), and culture supernatant was harvested 2–3 times weekly. Anti-CEA antibody was purified from culture supernatant by protein G chromatography (Amersham Biosciences, Uppsala, Sweden) by use of a Bio-Rad medium pressure chromatography system (Bio-Rad, Hercules, CA).

LS174T Adenocarcinoma Cells

LS174T human colon cancer cells (ATCC# CL-188, Manassas, VA), which are known to express CEA, were cultured in Minimum Essential Media (MEM) supplemented with 10% fetal bovine serum (Invitrogen, Grand Island, NY). Cells were detached by tapping culture flasks, suspended in sterile saline, counted, and used to establish xenografts.

Animals

Male athymic nude mice (20–25 g, 5–6 weeks old) were obtained from Harlan (Indianapolis, IN). Mice were housed in a sterile room, handled under aseptic conditions in a laminar hood, and fed autoclaved chow. 100 μL of LS174T cells in suspension ($\sim 5 \times 10^6$ cells) were injected s.c. into the right flank of the mice. Mice were monitored regularly to check for tumor growth and body weight. The tumor size was measured by vernier calipers, and tumor volume was defined by the standard formula; $l \times w^2/2$, where l represents the length of the longest diameter (mm) and where w represents the length of the axis perpendicular to l. All animal procedures were approved by the Institutional Animal Use and Care Committee of the University at Buffalo.

Pharmacokinetic Study

T84.66 was administered intravenously via penile vein injection to xenograft-bearing mice (starting

tumor volume 500–600 mm^3) and to control athymic mice at three dose levels: 1, 10, and 25 mg/kg ($n = 4$/group). Blood samples, 25 μL, were collected from the retro-orbital plexus using calibrated capillary pipettes (Drummond Scientific Company, Cat # 2-000-020) that were prerinsed with EDTA. Samples were collected at 1 h, 3 h, 8 h, 1 day, 2 days, 4 days, 7 days, 12 days, 21 days, and 35 days from control athymic mice and at 1 h, 3 h, 8 h, 1 day, 2 days, 4 days, 7 days, and 12 days from xenograft-bearing mice. Blood was centrifuged at 13,000 rpm for 3 min and the plasma fraction was separated and stored at −20°C.

ELISA Procedure

T84.66 concentrations in mouse plasma were determined by an ELISA method. Briefly, Nunc Maxisorp 96-well plates (model # 62409-002, VWR, Bridgeport, NJ) were coated with recombinant carcinoembryonic antigen (Protein Sciences Corporation, 400 ng/mL in 20 mM Na_2HPO_4, 250 μL/well) and incubated at 4°C overnight. Samples and standards (200 μL) were added in triplicate and incubated for 2 h at room temperature. Goat anti-mouse-fab alkaline phosphatase conjugate (Sigma, St. Louis, MO, Cat #A1682, 1:500 in PB-Tween, 100 μL/well) was added to the wells and allowed to incubate for 1 h at room temperature. P-nitro phenyl phosphate (Peirce, Rockford, IL, 4 mg/mL in diethanolamine buffer, pH 9.8, 0.2 mL) was added to each well and the change in absorbance at 405 nm with time was monitored using the kinetic mode of a microplate reader (Spectra Max 250, Molecular Devices, Sunnyvale, CA). Standards were prepared by diluting stock solutions of anti-CEA IgG to appropriate concentrations (25–200 ng/mL) using phosphate buffered saline (pH 7.4) and mouse plasma (1% final v/v). Standard curves were linear in this concentration range. Intra-assay and inter-assay recoveries were within 90–110% and the associated variability at the limit of quantification (25 ng/mL) was less than 15%. Of note, the assay has been validated for accurate recovery of anti-CEA IgG in the presence of soluble (e.g., "shed") CEA in plasma. CEA concentrations up to 5 ng/mL do not lead to significant alteration in the accuracy or precision of assay of T84.66 in mouse plasma samples. Additionally, in preliminary studies conducted with untreated mice bearing LS174T xenografts, no animals were found to exhibit plasma CEA concentrations greater than 2 ng/mL.

Data Analysis

Pharmacokinetic parameters of T84.66 were initially estimated by noncompartmental pharmacokinetic analysis using WinNonlin, version 5.0 (Pharsight Corporation, Palo Alto, CA). The area under the concentration time curve to the last observable point (AUC_{last}) was estimated by the trapezoidal rule. Terminal half-life ($t_{1/2}$) was obtained from the terminal linear portion of the concentration–time curves.

Mathematical Modeling

Our lab has previously published a PBPK model that describes the role of FcRn as a determinant of the plasma and tissue disposition of IgG.[25] In the present work, the basic PBPK model has been revised and extended to incorporate a target-mediated elimination component to characterize the influence of specific antigen–antibody interactions on antibody disposition. Organs and tissues included in the PBPK model are plasma, lung, liver, gut, spleen, heart, muscle, skin, kidneys, and tumor. These organs were connected in an anatomical manner, as shown in Figure 1. Each organ was further divided into vascular, endosomal, and interstitial compartments (Fig. 2a). The "endosomal" compartment represents the endosomal volume within the vascular endothelium of each tissue. The tumor compartment includes a cell-space region that contains the tumor-associated CEA (Fig. 2b). The model was constructed to allow interaction of T84.66 with a fraction of the total CEA in the tumor, consistent with limited accessibility of antibody to all regions of a solid tumor.

The model incorporates key features related to IgG disposition such as (i) uptake of IgG from the vascular layer and interstitial cell layer by fluid- phase endocytosis,[26–29] (ii) FcRn-mediated salvage of IgG in the endosomal layer of the endothelial cells in each organ,[30–32] (iii) elimination of unbound IgG from all organs,[31] (iv) convective transport of IgG via paracellular pores from the vascular to interstitial cell layer,[32–34] (v) the influence of CEA on antibody distribution and elimination, and (vi) transport of IgG from the interstitial space back to the systemic circulation via the lymphatic system.[32,34] In the previously

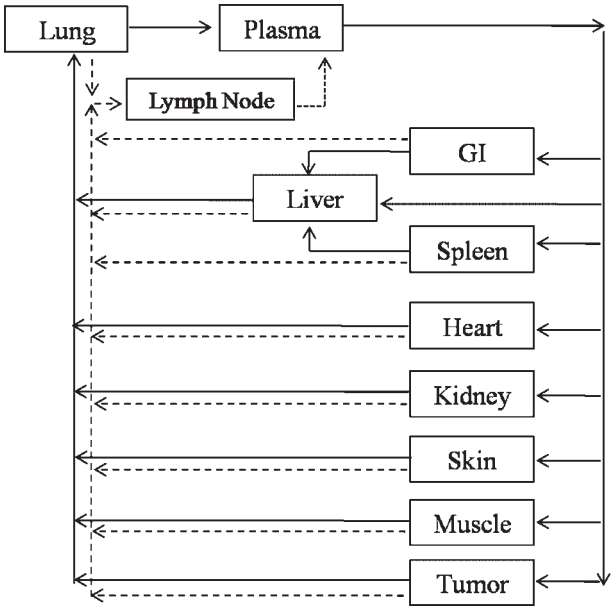

Figure 1. Physiologically based pharmacokinetic (PBPK) model of T84.66, monoclonal anti-CEA antibody disposition. All major organs are connected in an anatomical fashion with plasma flow represented by solid arrows and lymph flow by dashed arrows. Each organ compartment is divided into sub-compartments as shown in Figure 2.

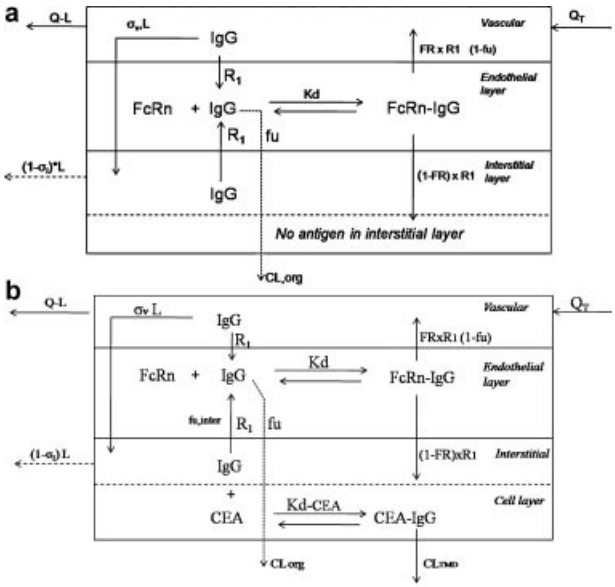

Figure 2. Intra-tissue sub-compartmental model for T84.66 disposition. (a) Nontumor tissues. Each organ in the model is divided into three sub-compartments representing a vascular space, an endothelial endosomal space, and interstitial space. Q and L represent the plasma and lymph flow rates. $\sigma_{V,organ}$ and $\sigma_{I,organ}$ are the vascular and lymphatic reflection coefficients, and R_1 is the rate of uptake and return of IgG from the vascular and interstitial compartments into the endosomal space. K_d is the dissociation constant for antibody binding to FcRn, which is present in the endosomal space of each organ. FR represents the fraction of FcRn-bound antibody that is recycled to the vascular space, and fu is the unbound fraction of antibody. CL_{organ} is the clearance of unbound IgG from the endosomal space of each organ. (b) Tumor tissue. The tumor compartment is divided into four sub-compartments comprising of the vascular space, an endothelial endosomal space, an interstitial space, and space associated with tumor cells. In addition to the parameters described for nontumor tissues, tumor parameters include the equilibrium dissociation constant for IgG-CEA binding ($K_{d\text{-}CEA}$), the fraction of IgG not bound to CEA (fu_{inter}), and the clearance of the IgG bound to CEA (CL_{TMD}).

published model, the lymph outflow from the interstitial layer of each organ was assumed to drain directly into the plasma compartment. In the present model, we have incorporated a transit compartment to represent lymph nodes, which collect the lymphatic drainage from all organs before returning lymph fluid to the systemic circulation. The parameters and variables used in the model are defined in Appendix I and the equations for the model are provided in Appendix II.

Shown below is a representative mass balance equation for the vascular compartment within an organ:

$$\begin{aligned} V^{V}_{organ}\frac{dC^{V}_{organ}}{dt} &= (Q_{organ}\times C_{plasma}) \\ &+ ((FR\times R_1\times(1-fu_{organ}))\times C^{Total}_{EndoOrgan} \\ &\times V^{E}_{organ}) - (R_1\times C^{V}_{organ}\times V^{V}_{organ}) \\ &- ((1-\sigma^{V}_{organ})\times L_{organ}\times C^{V}_{organ}) \\ &- ((Q_{organ}-L_{organ})\times C^{V}_{organ}) \end{aligned}$$

In this equation, Q_{organ} is the blood flow to the vascular compartment and C_{plasma} refers to the antibody concentration in plasma. The fraction of antibody bound ($1-fu_{organ}$) to the FcRn receptor is returned to the vascular compartment by rate constant R_1. IgG in the vascular space may be taken up into the endosomal compartment by the rate constant R_1, and vascular IgG may be transported to the interstitial space of the organ via convection, as determined by the vascular reflection coefficient ($\sigma_{V,organ}$) and the flow rate of

lymph fluid (L_{organ}). IgG may also exit the vascular compartment via blood flow returning back to systemic circulation, where the plasma flow out of the organ is equal to the plasma flow into the organ minus the lymph flow rate ($Q_{organ} - L_{organ}$).

Model Parameters

The physiological parameters for plasma flow rates and vascular, interstitial and total organ volumes were obtained from the literature.[35] The lymph flow rates were set to 2% for visceral organs and 4% for muscle and skin.[33] Endosomal volumes for each organ was fixed to 0.5% of total organ volume.[25] The equilibrium dissociation constant for IgG binding to FcRn was obtained from the literature.[36] The vascular reflection coefficient and lymph reflection coefficient values were set to 0.95 and 0.2.[25] These values were assumed to be the same for all organs. Endogenous antibody production was assumed to occur by a zero-order rate process, K_0. The value for this parameter, 1.63×10^{-12} M/min, was defined through an iterative process, where K_0 was adjusted to achieve a steady-state plasma concentration of endogenous IgG of 14.7 μM. Also through this process, the model structure was used to define steady-state endogenous IgG concentrations in all model compartments, and these values were used in subsequent modeling work as the "initial conditions" of all differential equations for endogenous IgG.

IgG clearance from each organ was calculated based on total intrinsic clearance values obtained from a mechanistic model previously developed in our laboratory.[37] Individual organ clearances were obtained by fractioning the total clearance into organ clearances based on the tissue size.

Based on our previous model, the estimated value for the rate of uptake into the endosomal compartment (R_1) and rate of recycling (R_2) were 1.96 (1/day) and 20.4 (1/day), respectively. Since the rate of recycling appears to be extremely fast compared to the uptake rate, we decided to use a single unifying rate constant, R_1 to describe the uptake of IgG into the endosomal compartment and its return back to the vascular compartment. The value for the rate constant R_1 was obtained by fitting the PBPK model to T84.66 plasma concentration data from control mice. The value for the recycling fraction (FR) was fixed at 0.715 based on our previous model, and the volume for the lymph node compartment was assumed to be equal to volume of spleen.[38] An estimate for transit time associated with the lymph node (Tau) was not available from the literature, and was obtained by fitting the PBPK model to the T84.66 plasma concentration data.

Parameters for the Tumor Compartment

The rate of plasma flow to the tumor was obtained from literature,[32] and the tumor lymph flow rate was set to 4% of the plasma flow rate. The total tumor volume was defined through the use of an exponential growth function, based on *in vivo* measurements of tumor growth (Fig. 3). Tumor volume at any given time (TV_t) was defined as the initial tumor volume, TV_0, multiplied by $\exp((0.0000635 \times \text{time}))$. Relative to the total tumor volume, the vascular volume was fixed at 7%, the interstitial volume at 55%,[32] and the endosomal volume was fixed at 0.5%. The lymph reflection coefficient was fixed to 0.2. Given that tumor vasculature has been noted to be more heterogeneous and more porous than vessels associated with healthy tissues, we expect that the value for tumor reflection coefficient (σ_{tumor}) would be lower than the reflection coefficient associated with normal tissues. σ_{tumor}

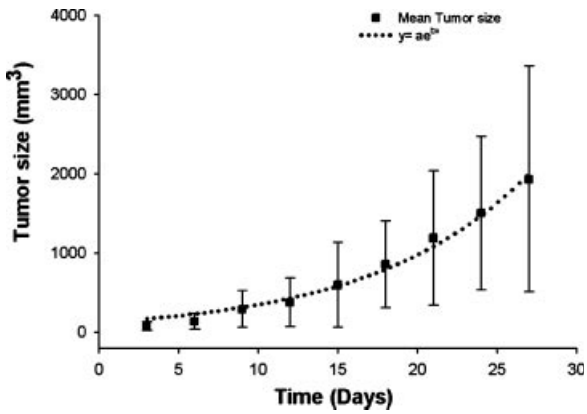

Figure 3. LS174T tumor growth curve. The increase in tumor volume with time was captured with an exponential growth function, $y = a\,e^{bx}$, where y = tumor tumor volume, a = initial tumor volume, x = time of measurement, and b = exponent of tumor growth. The fit growth function was used in the PBPK model to increase tumor compartment volumes as a function of time. All other tumor parameters were either constant with tumor volume (e.g., $\sigma_{V,organ}$, $\sigma_{I,organ}$, etc.) or set as a fixed function of tumor volume (e.g., FcRn mediated organ clearance, CL_{organ}).

was estimated from plasma data obtained in tumor bearing mice.

The dissociation constant for IgG interaction with CEA was fixed at 3.8×10^{-11} M,[24] and the concentration of CEA in the tumor compartment was fixed at 110 μg/g.[39] The influence of CEA on the clearance of T84.66 was modeled such that T84.66 bound to CEA would be available for target-mediated elimination, and unbound T84.66 would be available for removal from the tumor via the outflow of lymph fluid. Several studies previously published in the literature suggest that antibodies directed against tumor associated antigens may not distribute homogenously due to transport barriers, heterogeneous distribution of tumor associated antigens,[40] and due to a possible "binding-site barrier."[41] To account for limited accessibility of CEA to T84.66 in the interstitial fluid of the tumor, an accessibility parameter (FA) was incorporated into the model, and estimated by fitting to the observed concentration data. The fraction of antibody unbound to FcRn (fu_{organ}) and the total antibody concentration in the endosomal space are defined by Eqs. (15)–(17) in Appendix II. The fraction of antibody in the tumor interstitial space that is not bound to CEA (fu_{inter}) is defined by Eqs. (18) and (19) in Appendix II. Table 1 lists the parameters used in the model and provides references to any literature sources.

Parameter Estimation

Unknown model parameters were R_1, the rate constant of uptake and return of IgG from the endosomal space, and Tau, the transit time associated with lymphatic transit. These two unknown parameters were fitted to the plasma data obtained from control animals at three dose levels: 1, 10, and 25 mg/kg. The parameters were fit to the data sets simultaneously using maximum likelihood estimation of the ADAPT II program[43] with the following variance model:

$$\mathrm{Var}(t) = (\sigma_{\mathrm{inter}} + \sigma_{\mathrm{slope}} Y(t))^2$$

Y(t) is the model output at time t and Var(t) is the variance associated with the output. σ_{inter} and σ_{slope} are the two variance parameters representing a linear relationship between the SD of the model output and $Y(t)$.

Parameter values for R_1 and Tau were then fixed, and unknown parameters associated with the tumor compartment were fitted. Unknown tumor parameters were the clearance of T84.66 bound to tumor antigens (CL_{TMD}), the CEA accessibility parameter for antibody–antigen interaction (FA), and the reflection coefficient for the tumor vascular space (σ_{tumor}). Parameters were estimated with simultaneous fitting to plasma data obtained from LS174T xenograft-bearing mice, using data from three dose levels (1, 10, and 25 mg/kg), and using weighted least

Table 1. Parameters Used for Modeling IgG Plasma Concentrations in Control Foxnu and LS174T Xenograft Bearing Mice

Parameter (Units)	Plasma Flow[a] (mL/min)	Lymph Flow[b] (mL/min)	Total Volume[a] (mL)	Vascular Volume[a] (mL)	Interstitial Volume[a] (mL)	Endosomal Volume[c] (mL)	Organ Clearance[d] (mL/min)
Plasma			0.774				
Lung	4.16	0.0842	0.191	0.0191	0.057	9.55E−04	1.43E−06
GI	0.9	0.018	3.45	0.10	0.600	1.73E−02	2.58E−05
Liver	1.1	0.022	0.951	0.095	0.190	4.76E−03	7.10E−06
Spleen	0.05	0.001	0.10	0.010	0.020	5.00E−04	7.47E−07
Heart	0.28	0.0056	0.133	0.007	0.019	6.65E−04	9.93E−07
Kidney	0.80	0.016	0.298	0.03	0.101	1.49E−03	2.22E−06
Skin	1.21	0.0484	2.94	0.20	0.999	1.47E−02	2.19E−05
Muscle	0.80	0.032	7.924	0.15	1.032	3.96E−02	5.92E−05
Tumor	0.10	0.004	Function of tumor growth				

[a]From Baxter et al.[32]
[b]From Covell et al.[33]
[c]Assumed to be 0.5% of tissue volume.
[d]From Hansen and Balthasar.[42]

squares estimation of ADAPT II program.[43] Each observation was weighted to inverse of the variance of the output error ($1/\sigma^2$).

Sensitivity Analysis

The sensitivity of model output to model parameters was assessed by evaluating the percentage change in plasma AUC with the alteration of model parameters by ±10%:

$$\%\text{Change} = \frac{\text{AUC}_{\text{SIM}} - \text{AUC}_{\pm 10\%}}{\text{AUC}_{\text{SIM}}} \times 100$$

AUC_{SIM} refers to the AUC obtained with the optimized parameters and $\text{AUC}_{\pm 10\%}$ is the AUC obtained following a 10% increase or decrease in the parameter value.[44] The analyses were performed with simulated administration of 25 mg/kg T84.66.

Model Evaluation

To test the prediction capability of the PBPK model, tumor concentrations of T84.66 were determined in a separate study following administration of 1 and 10 mg/kg doses of radiolabeled T84.66. Observed tumor concentrations were compared with model simulated values.

T84.66 was labeled with Iodine-125 (Perkin Elmer Life & Analytical Sciences, Waltham, MA) using a modified Chloramine-T method.[45] Briefly, 10 μL of ^{125}I (100 mCi/mL) was added to 40 μL of T84.66 (~1 mg/mL in phosphate buffered saline). The reaction was initiated by addition of 20 μL of 1 mg/mL chloramine-T in phosphate buffer. After 90 s, the reaction was stopped by addition of 25 μL sodium metabisulfite (2 mg/mL) in phosphate buffer followed by 40 μL of 10 mg/mL potassium iodide in double distilled water. The reaction mixture was lightly vortexed and immediately loaded on a Sephadex G-25M prepacked column (GE Healthcare, Uppsala, Sweden). Labeled antibody was collected in 500 μL fractions and 1 μL samples were obtained from each fraction to determine location of the labeled antibody peak. The labeled antibody was stored at 4°C until used.

The radiochemical purity of ^{125}I-IgG was determined by instant thin layer chromatography (ITLC). One microliter of radiolabeled anti-CEA IgG was spotted at the lower bottom end of the ITLC plate. Eighty-five percent methanol was used as the mobile phase for plate development and strips cut from the plate were read on a gamma counter. The percentage of bound ^{125}I was calculated from the quotient of radioactivity in the bottom section of the plate to the amount of radioactivity in the entire plate. Radiochemical purity of the labeled antibody preparation was greater than 98%.

T84.66 Tumor Concentrations in Mice

LS174T xenografts were established in male athymic nude mice as described above. Two days before administration of ^{125}I–T84.66, study animals were given potassium iodide (0.2 g/L) in their autoclaved drinking water to block the thyroid uptake of ^{125}I. ^{125}I-labeled T84.66 was administered via penile vein injection to xenograft-bearing mice at 1 and 10 mg/kg (^{125}I activity ~10 μCi/mouse) to 6 mice per dose level. At 30 min and 7 days following T84.66 administration, groups of three mice from each dose group were sacrificed. Blood was obtained by cardiac puncture, and tumor tissue was excised and weighed in plastic culture tubes. Radioactive counts were determined by gamma counting, and corrected for background and decay.

RESULTS

T84.66 plasma pharmacokinetics were studied at 1, 10, and 25 mg/kg dose levels in control and LS174T adenocarcinoma-bearing Fox^{nu} athymic mice. T84.66 clearance in control mice at 1, 10, and 25 mg/kg was 0.181 ± 0.097, 0.283 ± 0.051, and 0.211 ± 0.056 mL/h/kg. ANOVA did not identify significant differences between these clearance values ($p > 0.05$). PBPK model parameters R_1 and Tau were fit to the plasma data obtained from the three doses (simultaneously). The model provided good fits for the control plasma data at all doses as shown in Figure 4, and the best fit values of the parameters with the associated CV% were R_1: 0.715 day^{-1} (0.112%) and Tau: 2.12 h (10%).

In xenograft-bearing mice, T84.66 doses of 1, 10, and 25 mg/kg were associated with time-averaged clearance values of 1.40 ± 0.23, 0.977 ± 0.19, and 0.973 ± 0.33 mL/h/kg, respectively. At each dose level, clearance was significantly greater than the clearance observed at the corresponding dose in control mice ($p < 0.05$).

The three unknown parameters of the tumor model, that is, the vascular reflection coefficient of the tumor compartment (σ_{tumor}), clearance of

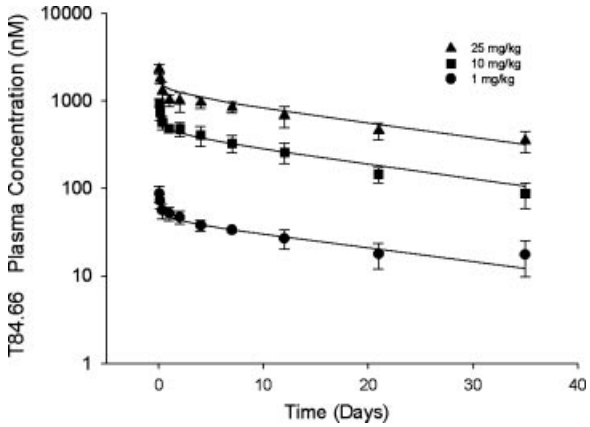

Figure 4. T84.66, anti-CEA antibody pharmacokinetics in mice. T84.66 was administered to Fox^{nu} athymic mice at three dose levels, 1 mg/kg (circles), 10 mg/kg (squares), and 25 mg/kg (triangles). Unknown model parameters, R_1 and Tau, were fit to all data sets simultaneously. Solid lines denote the best fit obtained from the PBPK model. Each symbol represents the mean concentration, and error bars indicate the standard deviation ($n = 4$).

anti-CEA IgG due to specific binding to CEA (CL_{TMD}), and the CEA accessibility parameter (FA, which represents the fraction of CEA available for binding to antibody), were estimated with good precision. The best-fit values were σ_{tumor}: 0.842 (0.374%), CL_{TMD}: 0.166 mL/min (5.33%), and FA: 0.203 (3.95%). The final model provided good characterization of the data obtained from all dose-levels administered in control and tumor-bearing mice (Fig. 5a–c). All estimated parameters and associated CV% values are listed in Table 2.

The model structure and parameters were employed to simulate the relationship of tumor and plasma concentrations, to predict the extent of binding of tumor CEA to antibody (i.e., receptor occupation), and to determine the contribution of CEA-mediated clearance of T84.66 to the total elimination of the antibody. The percent contribution of CEA-mediated elimination of T84.66 decreased from 86% at the 1 mg/kg dose to 81% and 65% at the 10 and 25 mg/kg doses, respectively. As such, the contribution of the target mediated clearance pathway was greatest at the lowest dose, consistent with increased saturation of CEA with increasing doses. Figure 6 presents model-simulated dose-normalized plasma T84.66 concentrations in tumor bearing mice and control mice, facilitating the visualization of the dose dependency in T84.66 pharmacokinetics. The time-course of tumor to plasma T84.66 concentration ratios, following simulated doses of 1, 10, and 25 mg/kg, are shown in Figure 7. Due to relatively slow entry of antibody into the tumor interstitial fluid, and due to rapid CEA-mediated clearance, the model predicts a low ratio of tumor to blood concentrations of antibody. Interestingly, the highest dose of T84.66, 25 mg/kg, was predicted to lead to the highest tumor:blood concentration ratio at early time points relative to dosing. This prediction, which is opposite of the intuitive expectation for decreased tumor selectivity with increasing dose or concentration (due saturation of antibody binding to CEA), is indicating that CEA-mediated clearance of T84.66 from tumor is playing the dominant role in determining T84.66 tumor concentrations. At high concentrations, where CEA-T84.66 binding is saturated, CEA-mediated clearance is less efficient, and this leads to higher tumor:blood concentration ratios.

Sensitivity Analysis

A sensitivity analysis was conducted to determine the parameters to which the T84.66 plasma concentration output is most sensitive. The results from the sensitivity analysis were based on the percent change in the area under the plasma concentration curve (AUC) for T84.66 following a simulated 25 mg/kg dose (Fig. 8). Small absolute values for percent change in AUC indicate insensitivity to that parameter; negative values for percent change indicate a decrease in plasma AUC with an increase in the parameter. The sensitivity analysis showed that the vascular reflection coefficient ($\sigma_{V,organ}$), tumor vascular reflection coefficient (σ_{tumor}), concentration of tumor associated antigen CEA (nPt_{CEA}), antigen accessibility parameter (FA) and total tumor volume (V_{tumor}) were key parameters influencing plasma antibody concentration. Moderate sensitivity was observed for the parameters representing blood flow to the tumor compartment (Q_{tumor}), clearance of CEA-T84.66 complexes (CL_{TMD}), lymph flow transit time (Tau), the lymphatic reflection coefficient ($\sigma_{I,organ}$), the rate constant for IgG uptake into the endosomal compartment (R_1), tissue FcRn concentration (nPt_{organ}), and the antibody recycling fraction (FR). Plasma antibody concentrations were relatively insensitive to changes in dissociation constant for IgG-FcRn binding (K_d) and IgG-CEA binding ($K_{d\text{-}CEA}$).

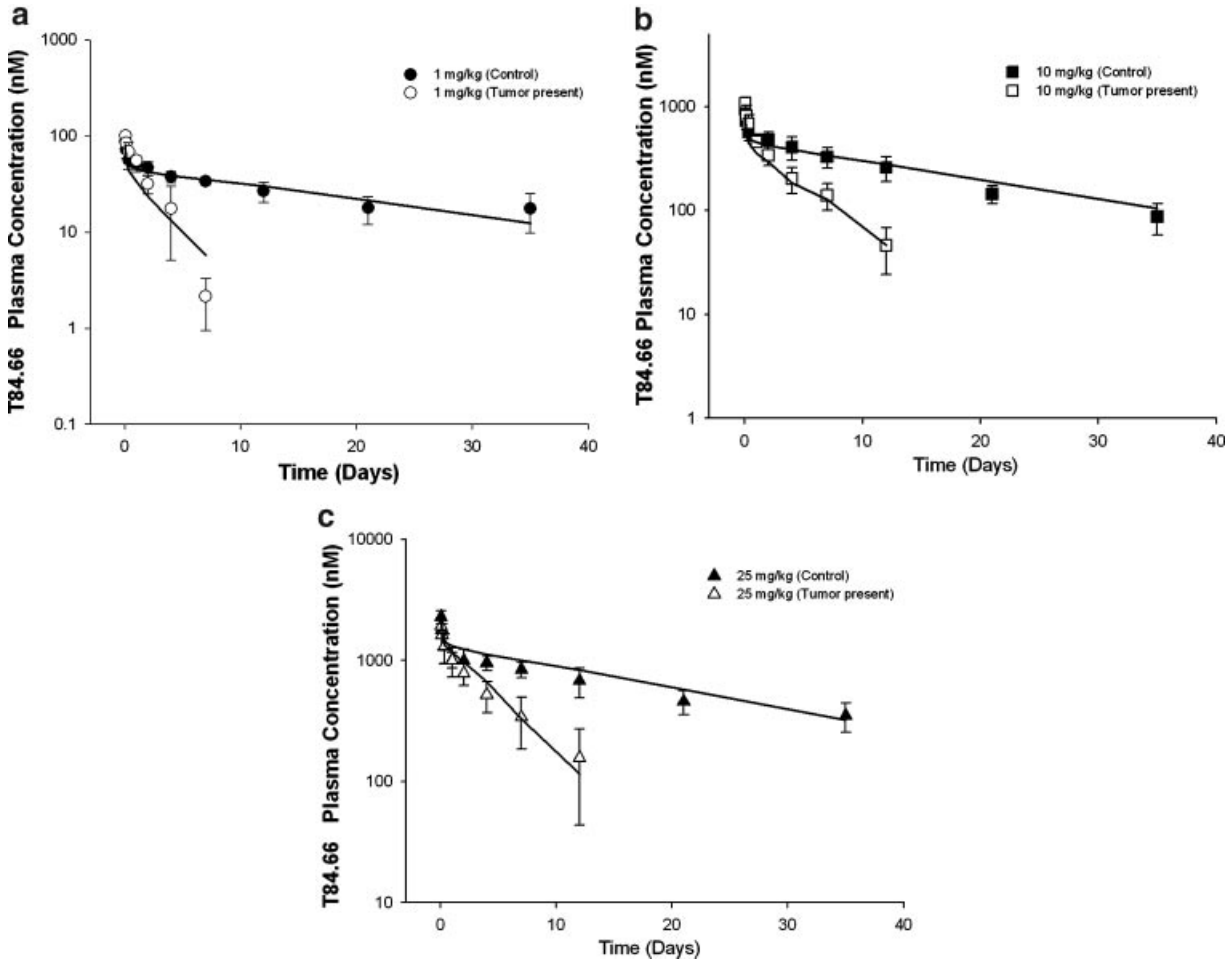

Figure 5. Comparison of T84.66 disposition in control and LS174T xenograft-bearing mice. (a) Solid circles represent plasma T84.66 concentration data collected from control mice and open circles represent mean data obtained from tumor bearing mice following intravenous administration of 1 mg/kg T84.66. (b) Solid squares represent plasma T84.66 concentration data collected from control mice and open squares represent mean data obtained from tumor bearing mice following intravenous administration of 10 mg/kg T84.66. (c) Solid triangles represent plasma T84.66 concentration data collected from control mice and open triangles represent mean data obtained from tumor bearing mice following intravenous administration of 25 mg/kg T84.66. The solid lines represent the best fit obtained from the PBPK model. Each symbol represents mean plasma concentrations, as measured by ELISA, and error bars indicate standard deviations associated with each mean ($n = 3$–4).

Model Evaluation: Comparison of Model Simulated Tumor T84.66 Concentrations With Observed Data

The physiologically based pharmacokinetic (PBPK) model was developed based on plasma concentrations of T84.66 obtained following antibody administration to mice with or without CEA-expressing LS174T xenografts. Antibody concentrations in tissues, including tumor tissue, were not available, and model fitting was based solely through the use of plasma data. To evaluate the predictive capability of the PBPK model, tumor concentrations were determined following administration of T84.66, at doses of 1 and 10 mg/kg, in a separate model evaluation experiment. As shown in Figure 9, the observed data were in good agreement with the model predictions at the time points studied (30 min and 7 days). T84.66 concentrations in other tissues were not determined.

Table 2. Parameters Estimated from the PBPK Model

Parameter	Model Estimates (%CV)
FR	0.715_f
Parameters associated with basic PBPK model	
Tau (h)	2.12_e (0.122)
R_1 (1/day)	0.715_e (10.0)
Parameter associated with tumor compartment	
CL_{TMD} (mL/min)	0.166_e (0.374)
FA	0.203_e (5.33)
σ_{tumor}	0.842_e (3.95)

f, parameter value fixed to estimate obtained from Garg and Balthasar.[25] e, parameters estimated in current model.

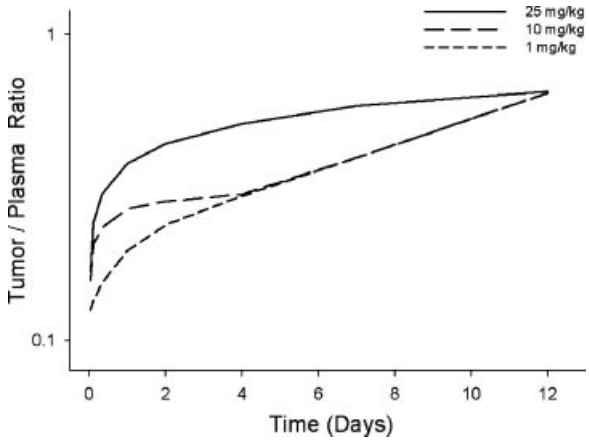

Figure 7. Comparison of simulated tumor-to-plasma ratios of T84.66 at 1, 10, and 25 mg/kg dose levels. Model predictions are indicated with the short dashed line (1 mg/kg dose), the long dashed line (10 mg/kg), and with the solid line (25 mg/kg).

DISCUSSION

Antibodies are capable of selectively targeting tumor-associated antigens, and antibodies are being increasingly used for the treatment of various cancers. Saturable binding of antibody with target antigen will lead to dose-dependencies and time-dependencies in the site-selectivity of antibody distribution, complicating efforts to select dosing protocols that would provide the greatest ratio of therapeutic benefit versus off-site toxicity. Model-based approaches for dose-selection have not come into common use, as few mechanistic models have been published to allow the prediction or characterization of the effect of antigen binding and target-mediated elimination on the tissue-selectivity of antibody disposition.[38,46–48] The present work was undertaken to extend our previous model of antibody disposition, which accounts for the effects of FcRn on IgG distribution and elimination, to incorporate effects associated with specific binding to target antigens. T84.66, a murine monoclonal anti-CEA

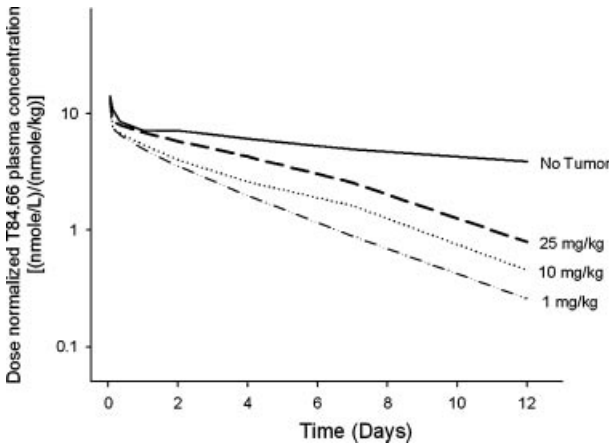

Figure 6. Dose normalized concentration time profile of T84.66 in the mice with or without LS174T xenografts. The solid line represents model simulated data for control mice (25 mg/kg dose level), and the dashed-dotted line indicates the model simulation for the 1 mg/kg dose level in xenograft-bearing mice. Model simulations for the 10 and 25 mg/kg doses, in tumor bearing mice, are denoted by the dotted line and long dashed line, respectively.

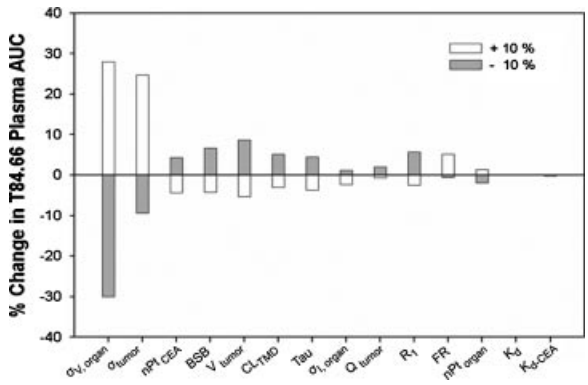

Figure 8. Sensitivity analyses. The plots represent the percent change in area under the T84.66 plasma concentration time profile following ±10% changes selected parameter values. Small changes in model output indicate that plasma exposure is relatively insensitive to the adjusted parameter. Negative values indicate a decrease in model output with increases in the adjusted parameter. Symbols used along *x*-axis have been included in Appendix I.

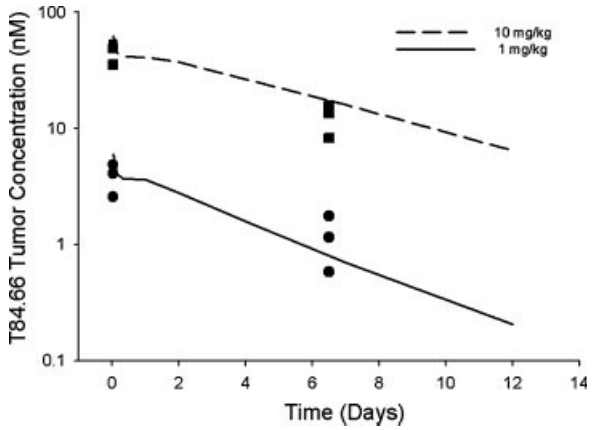

Figure 9. Comparison of PBPK model-predicted versus observed tumor concentration. Simulations were conducted to predict antibody concentrations in tumor tissue following T84.66 doses of 1 and 10 mg/kg in LS174T xenograft-bearing mice. Experimental data were then obtained following administration of ^{125}I-T84.66, with tumor concentrations determined via gamma counting. Solid line represents model predictions at 1 mg/kg dose and dashed line is the model predication at the 10 mg/kg dose. Data obtained from individual mice are shown as closed symbols.

IgG antibody, and LS174T, a human adenocarcinoma that expresses CEA, were selected for investigation.

In control animals that do not harbor LS174T tumors, T84.66 exhibited linear elimination and dose-proportional increases in plasma concentration over the dose-range of 1–25 mg/kg (Fig. 3). In animals bearing LS174T tumors, T84.66 time-averaged clearance was increased several fold, consistent with target-mediated antibody elimination (Fig. 5a–c).

Our previous PBPK model demonstrated the importance of FcRn expressed in various tissues such as skin, muscle, liver, gastrointestinal tract and the kidneys on antibody pharmacokinetics. This model was able to capture the plasma pharmacokinetics of 7E3, a monoclonal IgG antibody, reasonably well.[25] Of note, 7E3 is directed against human glycoprotein IIb/IIIa, and the mAb has no known specific binding target in mice. Although the model provided good characterization of the 7E3 data, there was some disagreement between the model predictions and observed values, especially at the initial time points. Similarly, the prior PBPK model over-predicted T84.66 concentrations in control mice lacking the tumor antigen. This prior PBPK model assumes that antibody from interstitial compartment is directly returned to the systemic circulation by lymphatic drainage. This assumption may not be completely valid, since it is known that lymph outflow accumulates in the lymph nodes before gaining access to the blood circulation. To improve model performance, a lymph node transit compartment was incorporated. The transit time for antibody movement through this lymph compartment was characterized with the parameter Tau, which was estimated to be 2.12 ± 0.21 h. Inclusion of this parameter allowed excellent characterization of data obtained from tumor-free animals (Fig. 4).

To account for the increased clearance of T84.66 in tumor-bearing animals, a target mediated disposition component was incorporated into the model. We assumed that the presence of the tumor did not alter any of the physiological determinants of antibody disposition (e.g., tissue volumes, blood flow, convective transport, FcRn processing, etc.). Differences in antibody disposition between control and tumor-bearing animals were assumed to result from antibody binding to antigen, and by the elimination of antibody bound to antigen in tumor tissue. To account for tumor growth following inoculation of tumor cells (Fig. 3), the volumes of each tumor sub-compartment were increased with time, using an exponential growth function.

It is recognized that CEA that is shed from the xenograft into the serum might lead to immune complex formation with T84.66, thereby influencing the pharmacokinetics of T84.66. However, plasma collected from the tumor bearing mice revealed CEA concentrations below the limit of quantification for our assay, 2 ng/mL ($\sim$0.01 nM), which is far lower than the concentrations of T84.66 observed at all time points, after each dose of antibody. As such, shed CEA is not likely to be a significant determinant of T84.66 disposition in the LS174T xenograft model. Anti-drug antibodies (ADA), generated against therapeutic mab, may be important determinants of antibody pharmacokinetics. ADA and therapeutic antibodies may form complexes *in vivo*, leading to rapid drug elimination via complement and/or Fc-gamma-receptor pathways. The development of an ADA response is thought to depend on the nature of the dosing regimen (with greater ADA development with chronic dosing), the immune status of the recipient, the extent of similarity between host immunoglobulin and

the therapeutic antibody, and the route of drug administration (i.e., with greater ADA response expected for SC dosing vs. IM dosing vs. IV dosing). The extent of complexation and the complex clearance rate are known to depend on the size of immune complex formed, the concentration of the drug, the concentrations of anti-drug antibodies, and on the kinetics and stoichiometry of interaction between therapeutic antibody and anti-drug antibodies.[49] Although not measured, it is expected that there was little or no ADA development in this study, as T84.66, a mouse monoclonal antibody, was administered to immuno-compromised nude mice as a single, IV dose. Due to our expectations for minimal potential for significant interaction between soluble CEA and T84.66, and due to our expectations for a very low likelihood for development of an anti-T84.66 antibody response, the model presented in this article has not included a pathway for immune-complex mediated elimination of anti-CEA antibody.

The model was able to capture the accelerated clearance of T84.66 from plasma in the presence of CEA-positive xenografts. The CV% of the parameters associated with the tumor compartment, namely σ_{tumor}, CL_{TMD}, and FA, were less than 6%. The estimated value of tumor vascular reflection coefficient σ_{tumor} was 0.842, which is less than the value assumed for all other tissues ($\sigma_{V,organ}$: 0.95). This parameter estimate is consistent with the expectation that the tumor vasculature will be highly permeable due to local secretion of various vascular permeability enhancers, such as vascular endothelial growth factor. Also, tumor vessels are known to be dilated and leakier due to the loss of the normal, continuous arrangement of vascular cells in the tumor wall, thereby providing decreased resistance to antibody uptake into the interstitial compartment.

Sensitivity analyses indicate that the vascular coefficient is indeed a very important parameter governing plasma antibody concentrations. Additionally, tumor associated antigen concentration and tumor antigen accessibility were important determinants of plasma IgG concentration. This is in accordance with published literature reports which suggest that antigen distribution across a tumor surface can be extremely heterogeneous and successful antibody antigen binding can also impede antibody transport.[40,41] Importantly, the model was less sensitive to parameters associated with IgG binding to FcRn (e.g., FcRn concentration and the recycling fraction of IgG from the endosomal compartment). This implies that in the presence of a significant target mediated elimination pathway, FcRn plays a minor role in determining antibody disposition.

Other models describing IgG pharmacokinetics in the presence of tumor have been published in the literature. Baxter et al.[32] compared the pharmacokinetics of a tumor-specific antibody in xenograft bearing mice with that of a nonspecific antibody. This model, however, does not consider the role of FcRn in protecting IgG from elimination and cannot account for the influence of endogenous IgG concentrations and IgG-FcRn binding affinity on antibody kinetics. In their model, Baxter and Jain found that the tumor did not significantly influence antibody pharmacokinetics. However, Halpern et al.,[50] using the same tumor model, demonstrated a faster initial loss of the intact antibody from the blood of tumor bearing mice compared to normal mice. This difference in observations with the same tumor model could be due to various factors such as the specific antibody used, binding affinity, antigen density, antigen shedding, size of tumor and the time course of study. Also, the affinity of the specific antibody to other antigens in normal organs could greatly influence the pharmacokinetics. Ferl et al.[51,52] published two articles studying the influence of FcRn on pharmacokinetics of an anti-carcinoembryonic antibody and a single-chain Fv antibody fragment. However, they did not compare the pharmacokinetics of the intact antibody in tumor bearing and control mice, limiting their ability to investigate the influence of antigen binding on anti-CEA antibody disposition.

Due to complexities associated with the processes of antibody distribution (e.g., determinants of convection) and due to target-mediated elimination, it is often difficult to predict, a priori, dose requirements for monoclonal antibodies to achieve desired levels of target saturation. For small molecule drugs, it is typical to assume that drug distribution is predominantly controlled by diffusion, and that steady-state unbound concentrations of drug in plasma will be equivalent to steady-state unbound drug concentrations in tissues. As such, simple consideration of input rate, plasma clearance, and receptor affinity often allows useful projection of relationships between dosage rates and receptor occupation. However, in the case of macromolecule drugs, such as antibodies, the efficiency of uptake into

tissue via convection is much lower than the efficiency of drug elimination from tissue via convection. As such, drug concentration in tissue interstitial fluid is typically much lower than drug concentrations in plasma. Additionally, when the macromolecule is subject to target-mediated elimination, steady-state tissue interstitial fluid concentrations may be further reduced relative to plasma concentrations, potentially by several logs. This lack of equivalence between drug concentration in plasma and drug concentrations in tissue fluid surrounding the target receptor (i.e., the biophase) greatly complicates efforts to predict dose levels of antibody to produce a desired level of receptor occupancy or effect.

Target-mediated disposition models are structured to allow consideration of the interaction of drug with the target receptor, and such models have been extremely useful in characterizing the effect of drug–target interaction on nonlinear drug distribution and elimination. However, the initial, general target-mediated elimination models assumed that the target receptor is accessible by drug in blood and, consequently, the simple target-mediated disposition models[13,48] do not consider the complex interplay between rates of antibody uptake into tissue, rates of antibody elimination via convection and catabolism, and receptor occupation. Conversely, PBPK models, as shown in this manuscript, are well-suited for consideration of the primary mechanisms associated with antibody disposition (e.g., convection, FcRn processing, target-mediated elimination), and provide an efficient means of predicting tissue concentrations and receptor occupation. For example, in this study, peak plasma T84.66 concentrations following the 1 mg/kg dose were more than 2000 times greater than the K_d for T84.66-CEA binding (i.e., ~90 nM vs. 0.038 nM). Despite the high concentrations of antibody in plasma, peak tumor concentrations were found to less than 10 nM, well below the concentration of CEA in tumor tissue (~600 nM). The concentration of T84.66 in tumor tissue, which is much lower than concentrations that would be anticipated based on consideration of plasma concentrations and receptor K_d, were well predicted by the physiologically based model. Consistent with the observed tumor concentration of T84.66, the model predicts that a 1 mg/kg IV dose of antibody will achieve a maximal receptor occupation of 0.32%, based on the model estimated quantity of accessible CEA (i.e., $FA \times nPt_{CEA}$), and a time-averaged receptor occupation of 0.14% for the time interval of 0–24 h. The model also predicts time-averaged occupation of 14.4% and 99.9% of the available CEA for the 10 and 25 mg/kg doses (0–24 h). It is important to note that the predictions, which would be impossible to make without the model structure, agree well with the observed tumor concentration data collected from the prospective model evaluation study (Fig. 9).

Although the PBPK structure provides many advantages, it is not very well suited for the investigation of inter-individual variability in antibody disposition following collection of sparse samples from large clinical studies. The PBPK model would allow mechanistic investigation of known or suspected determinants of inter-individual pharmacokinetic variability, perhaps including the "body load" of tumor, the extent of antigen expression on tumor tissue and on healthy tissue, vascular permeability, tumor blood flow, and rates of lymph flow.[53] However, due to the large number of parameters in the model, and due to the potential for inter-individual variability in each of the associated physiological processes, PBPK models are not likely to be useful for "population pharmacokinetic" analyses.

CONCLUSION

T84.66, a murine monoclonal IgG anti-CEA antibody, demonstrates rapid elimination in tumor bearing mice, consistent with target-mediated antibody elimination. The disposition of T84.66 in control and tumor-bearing mice was well described with a new PBPK model. This model will be used in future work to evaluate drug targeting strategies with T84.66, and the model may find application in predicting antibody disposition for inter-species scaling.

ACKNOWLEDGMENTS

This work was supported by grant CA114612 from the National Institutes of Health and by funding from Novartis Laboratories to the Laboratory for Protein Therapeutics of the University at Buffalo.

APPENDIX I

Section I: Parameters associated with the basic physiologically based pharmacokinetic model (NO TUMOR)

Parameter	Units	Definition
Q_{organ}	L/day	Plasma flow rate to each organ
$V^{\text{V}}_{\text{Organ}}$	L	Volume of vascular space
$V^{\text{E}}_{\text{Organ}}$	L	Volume of endosomal space
$V^{\text{I}}_{\text{Organ}}$	L	Volume of interstitial cell space layer
V_{plasma}	L	Mouse plasma volume
C_{plasma}	nM	Antibody concentration in plasma
$C^{\text{V}}_{\text{Organ}}$	nM	Antibody concentration in vascular space in each tissue
$C^{\text{E}}_{\text{Organ}}$	nM	Antibody concentration in endosomal space in each tissue
$C^{\text{I}}_{\text{Organ}}$	nM	Antibody concentration in interstitial cell space layer
$C^{\text{Total}}_{\text{Endo,Organ}}$	nM	Total antibody concentration in the endosomal space
CL_{organ}	L/day	Clearance of free antibody from endosomal layer
$n\text{Pt}_{\text{organ}}$	nM	FcRn concentration in each organ
FR		Recycling fraction of FcRn bound antibody
R_1	1/day	Endosomal uptake and return rate of antibody
$\sigma_{\text{V,organ}}$		Vascular reflection coefficient
$\sigma_{\text{I,organ}}$		Lymphatic reflection coefficient
L_{organ}	L/day	Lymph flow rate
K_{d}	nM	Dissociation constant for antibody FcRn binding
fu_{organ}		Unbound antibody fraction
Tau	day	Transit time for lymph transfer from lymph node to systemic circulation
X_{lymph}	nmol	Amount of antibody in the lymph node compartment
K_0	M/min	Endogenous antibody production rate

Section II: Additional parameters associated with the PBPK model in presence of tumor compartment

Parameter	Units	Definition
$K_{\text{d-CEA}}$	nM	Dissociation constant for antibody CEA binding
nPt_{CEA}	nM	CEA concentration in tumor cell space layer
FA		"Accessibility parameter" defines the fraction of antigen available for antibody binding
CL_{TMD}	L/min	Clearance of antibody bound to CEA from cell space layer

APPENDIX II: MODEL EQUATIONS

1. Plasma

$$V_{\text{Plasma}}\frac{dC_{\text{Plasma}}}{dt} = ((Q_{\text{lung}} - L_{\text{lung}}) \times C^{\text{V}}_{\text{lung}}) - ((L_{\text{gut}} + L_{\text{spleen}} + Q_{\text{liver}} + Q_{\text{heart}} + Q_{\text{kidney}} + Q_{\text{skin}} + Q_{\text{muscle}} + Q_{\text{tumor}}) \times C_{\text{plasma}}) + \left(\left(\frac{1}{\text{Tau}}\right) \times X_{\text{lymph}}\right) \quad (1)$$

2. Lung
   2.1 Vascular Space

$$V^{V}_{Lung}\frac{dC^{V}_{Lung}}{dt} = ((Q_{liver} - L_{liver}) \times C^{V}_{liver}) + ((Q_{heart} - L_{heart}) \times C^{V}_{heart}) + ((Q_{kidney} - L_{kidney}) \times C^{V}_{kidney}) + ((Q_{skin} - L_{skin}) \times C^{V}_{skin}) + ((Q_{muscle} - L_{muscle}) \times C^{V}_{muscle}) + ((Q_{tumor} - L_{tumor}) \times C^{V}_{tumor}) + (FR \times R_1 \times (1 - fu_{Lung}) \times C^{Total}_{EndoLung} \times V^{E}_{Lung}) - ((Q_{Lung} - L_{Lung}) \times C^{V}_{Lung}) - (R_1 \times C^{V}_{Lung} \times V^{V}_{Lung}) - ((1 - \sigma^{V}_{Lung}) \times L_{Lung} \times C^{V}_{Lung}) \quad (2)$$

   2.2 Endothelial Space

$$V^{E}_{Lung}\frac{dC^{Total}_{Endo,\,Lung}}{dt} = (R_1 \times C^{V}_{Lung} \times V^{V}_{Lung}) - (fu_{Lung} \times CL_{Lung} \times C^{Total}_{Endo\ Lung}) - ((1 - fu_{lung}) \times R_1 \times C^{Total}_{Endo\ Lung} \times V^{E}_{Lung}) + (R_1 \times C^{I}_{Lung} \times V^{I}_{Lung}) \quad (3)$$

   2.3 Interstitial Space

$$V^{I}_{Lung}\frac{dC^{I}_{Lung}}{dt} = ((1 - \sigma^{V}_{Lung}) \times L_{Lung} \times C^{V}_{Lung}) + ((1 - FR) \times R_1 \times (1 - fu_{Lung}) \times C^{Total}_{Endo\ Lung} \times V^{E}_{Lung}) - ((1 - \sigma^{I}_{Lung}) \times L_{Lung} \times C^{I}_{Lung}) - (R_1 \times C^{I}_{Lung} \times V^{I}_{Lung}) \quad (4)$$

3. Liver
   3.1 Vascular Space

$$V^{V}_{liver}\frac{dC^{V}_{liver}}{dt} = ((Q_{gut} - L_{gut}) \times C^{V}_{gut}) + ((Q_{spleen} - L_{spleen}) \times C^{V}_{spleen}) + ((Q_{liver} - Q_{gut} - Q_{spleen} + L_{gut} + L_{spleen}) \times C_{plasma}) + (FR \times R_1(1 - fu_{liver}) \times C^{Total}_{EndoLiver} \times V^{E}_{liver}) - (R_1 \times C^{V}_{liver} \times V^{V}_{liver}) - ((Q_{liver} - L_{liver}) \times C^{V}_{liver}) - ((1 - \sigma^{V}_{liver}) \times L_{liver} \times C^{V}_{liver}) \quad (5)$$

   3.2 Endothelial Space

$$V^{E}_{liver}\frac{dC^{E}_{liver}}{dt} = (R_1 \times C^{V}_{liver} \times V^{V}_{liver}) - (fu_{liver} \times CL_{liver} \times C^{Total}_{Endo\ Liver}) - ((1 - fu_{liver}) \times R_1 \times C^{Total}_{Endo\ Liver} \times V^{E}_{liver}) + (R_1 \times C^{I}_{liver} \times V^{I}_{liver}) \quad (6)$$

   3.3 Interstitial Space

$$V^{I}_{liver}\frac{dC^{I}_{liver}}{dt} = ((1 - \sigma^{V}_{liver}) \times L_{liver} \times C^{V}_{liver}) - ((1 - \sigma^{I}_{liver}) \times L_{liver} \times C^{I}_{liver}) + ((1 - FR) \times R_1 \times C^{Total}_{Endo\ Liver}) - (R_1 \times C^{I}_{liver} \times V^{I}_{liver}) \quad (7)$$

 DOI 10.1002/jps

4. Other Organs
   4.1 Vascular Space

$$V^{V}_{organ}\frac{dC^{V}_{organ}}{dt} = (Q_{organ} \times C_{plasma}) + ((FR \times R_1 \times (1 - fu_{organ})) \times C^{Total}_{EndoOrgan} \times V^{E}_{organ}) - (R_1 \times C^{V}_{organ} \times V^{V}_{organ}) - ((1 - \sigma^{V}_{organ}) \times L_{organ} \times C^{V}_{organ}) - ((Q_{organ} - L_{organ}) \times C^{V}_{organ}) \quad (8)$$

   4.2 Endosomal Space

$$V^{E}_{organ}\frac{dC^{Total}_{Endo,organ}}{dt} = (R_1 \times C^{V}_{organ} \times V^{V}_{organ}) - (fu_{organ} \times CL_{organ} \times C^{Total}_{EndoOrgan}) - ((1 - fu_{organ}) \times R_1 \times C^{Total}_{EndoOrgan} \times V^{E}_{organ}) + (R_1 \times C^{I}_{organ} \times V^{I}_{organ}) \quad (9)$$

   4.3 Interstitial Space

$$V^{I}_{organ}\frac{dC^{I}_{organ}}{dt} = ((1 - \sigma^{V}_{organ}) \times L_{organ} \times C^{V}_{organ}) - ((1 - \sigma^{I}_{organ}) \times L_{organ} \times C^{I}_{organ}) + ((1 - FR) \times R_1 \times (1 - fu_{organ}) \times C^{Total}_{endoOrgan} \times V^{E}_{organ}) - (R_1 \times C^{I}_{organ} \times V^{I}_{organ}) \quad (10)$$

5. Tumor Compartment
   5.1 Vascular Space

$$V^{V}_{tumor}\frac{dC^{V}_{tumor}}{dt} = (Q_{tumor} \times C_{plasma}) + ((FR \times R_1 \times (1 - fu_{tumor})) \times C^{Total}_{EndoTumor} \times V^{E}_{tumor}) - (R_1 \times C^{V}_{tumor} \times V^{V}_{tumor}) - ((1 - \sigma^{V}_{tumor}) \times L_{tumor} \times C^{V}_{tumor}) - ((Q_{tumor} - L_{tumor}) \times C^{V}_{tumor}) \quad (11)$$

   5.2 Endothelial Space

$$V^{E}_{tumor}\frac{dC^{Total}_{Endo,tumor}}{dt} = (R_1 \times C^{V}_{tumor} \times V^{V}_{tumor}) - (fu_{tumor} \times CL_{tumor} \times C^{Total}_{EndoTumor}) - ((1 - fu_{tumor}) \times R_1 \times C^{Total}_{EndoTumor} \times V^{E}_{tumor}) + (R_1 \times C^{I}_{tumor} \times fu_{inter} \times V^{I}_{tumor}) \quad (12)$$

   5.3 Interstitial Cell Space Layer

$$V^{I}_{tumor}\frac{dC^{I}_{tumor}}{dt} = ((1 - \sigma^{V}_{tumor}) \times L_{tumor} \times C^{V}_{tumor}) - ((1 - fu_{inter}) \times CL_{TMD} \times C^{I}_{tumor}) - ((1 - \sigma^{I}_{tumor}) \times L_{tumor} \times C^{I}_{tumor}) + ((1 - FR) \times R_1 \times (1 - fu_{tumor}) \times C^{Total}_{EndoTumor} \times V^{E}_{tumor}) - (R_1 \times C^{I}_{tumor} \times V^{I}_{tumor}) \quad (13)$$

6. Lymph Node Compartment

$$\frac{dx_{lymph}}{dt} = ((1 - \sigma^{I}_{lung}) \times L_{lung} \times C^{I}_{lung}) + ((1 - \sigma^{I}_{gut}) \times L_{gut} \times C^{I}_{gut}) + ((1 - \sigma^{I}_{spleen}) \times L_{spleen} \times C^{I}_{spleen}) + ((1 - \sigma^{I}_{liver}) \times L_{liver} \times C^{I}_{liver}) + ((1 - \sigma^{I}_{heart}) \times L_{heart} \times C^{I}_{heart}) + ((1 - \sigma^{I}_{kidney}) \times L_{kidney} \times C^{I}_{kidney}) + ((1 - \sigma^{I}_{skin}) \times L_{skin} \times C^{I}_{skin}) + ((1 - \sigma^{I}_{muscle}) \times L_{muscle} \times C^{I}_{muscle}) + ((1 - \sigma^{I}_{tumor}) \times L_{tumor} \times C^{I}_{tumor}) - \left(\left(\frac{1}{Tau}\right) \times X_{lymph}\right) \quad (14)$$

For each organ the unbound fraction (fu_{organ}) is defined as follows:

(1) Unbound fraction in endosomal layer:

$$fu_{organ} = 1 - \frac{1}{2 \times C^{Total}_{Endo,organ}} \times \left([Kd_{organ} + n Pt_{organ} + C^{Total}_{Endo,organ}] - \sqrt{(Kd_{organ} + n Pt_{organ} + C^{Total}_{Endo,organ})^2 - (4 \times C^{Total}_{Endo,organ} \times n Pt_{organ})} \right) \quad (15)$$

$$C^{Total}_{Endo,\ organ} = C^{Endogenous}_{Endo,\ organ} + C^{Anti-CEA}_{Endo,\ organ} \quad (16)$$

The relationship for fu_{organ} was based on the following equilibrium equation:[25]

$$IgG + FcRn \leftrightarrow FcRn - IgG; \qquad Kd_{organ} = \frac{[IgG]_u \times [FcRn]_u}{FcRn - IgG} \quad (17)$$

(2) Similarly the unbound fraction (fu_{inter}) in the interstitial layer of the tumor compartment is defined as follows:

$$fu_{inter} = 1 - \frac{1}{2 \times C^{Total}_{inter,tumor}} \times \left([Kd^{CEA}_{tumor} + (n Pt^{CEA}_{tumor} \times FA) + C_{Inter,tumor}] - \sqrt{(Kd^{CEA}_{tumor} + (n Pt^{CEA}_{tumor} \times FA) + C^{Total}_{Inter,\ tumor})^2 - (4 \times C^{Total}_{Inter,\ tumor} \times (n Pt^{CEA}_{tumor}) \times FA)} \right) \quad (18)$$

$$IgG + CEA \leftrightarrow CEA - IgG; \qquad Kd^{CEA}_{orgin} = \frac{[IgG]_u \times [CEA]_u}{CEA - IgG} \quad (19)$$

Eq. (18) is set up similar to Eq. (15) to determine the fraction of T84.66 unbound to the antigen CEA. The term ($n Pt^{CEA}_{tumor} \times FA$) denotes the fraction of carcinoembryonic antigen (CEA) available for binding to T84.66 IgG.

REFERENCES

1. Hebbar M, Tournigand C, Lledo G, Mabro M, Andre T, Louvet C, Aparicio T, Flesch M, Varette C, de Gramont A. 2006. Phase II trial alternating FOLFOX-6 and FOLFIRI regimens in second-line therapy of patients with metastatic colorectal cancer (FIREFOX study). Cancer Invest 24:154–159.
2. Tsipi Ben-Kasusa BS, Selaa M, Yardenb Y. 2007. Cancer therapeutic antibodies come of age: Targeting minimal residual disease. Mol Oncol 1:42–54.
3. Morell A, Terry WD, Waldmann TA. 1970. Metabolic properties of IgG subclasses in man. J Clin Invest 49:673–680.
4. Waldmann TA, Strober W. 1969. Metabolism of immunoglobulins. Prog Allergy 13:1–110.
5. Brambell FW, Hemmings WA, Morris IG. 1964. A theoretical model of gamma-globulin catabolism. Nature 203:1352–1354.
6. Waldmann TA, Jones EA. 1972. The role of cell-surface receptors in the transport and catabolism of immunoglobulins. Ciba Found Symp 9:5–23.
7. Simister NE, Mostov KE. 1989. Cloning and expression of the neonatal rat intestinal Fc receptor, a major histocompatibility complex class I antigen homolog. Cold Spring Harb Symp Quant Biol 54: 571–580.
8. Israel EJ, Wilsker DF, Hayes KC, Schoenfeld D, Simister NE. 1996. Increased clearance of IgG in mice that lack beta 2-microglobulin: Possible protective role of FcRn. Immunology 89:573–578.
9. Junghans RP, Anderson CL. 1996. The protection receptor for IgG catabolism is the beta2-microglobulin-containing neonatal intestinal transport receptor. Proc Natl Acad Sci USA 93:5512–5516.
10. Ghetie V, Hubbard JG, Kim JK, Tsen MF, Lee Y, Ward ES. 1996. Abnormally short serum half-lives of IgG in beta 2-microglobulin-deficient mice. Eur J Immunol 26:690–696.

11. Tabrizi MA, Tseng CM, Roskos LK. 2006. Elimination mechanisms of therapeutic monoclonal antibodies. Drug Discov Today 11:81–88.
12. Mager DE, Jusko WJ. 2001. General pharmacokinetic model for drugs exhibiting target-mediated drug disposition. J Pharmacokinet Pharmacodyn 28:507–532.
13. Coffey GP, Fox JA, Pippig S, Palmieri S, Reitz B, Gonzales M, Bakshi A, Padilla-Eagar J, Fielder PJ. 2005. Tissue distribution and receptor-mediated clearance of anti-CD11a antibody in mice. Drug Metab Dispos 33:623–629.
14. Gold P, Freedman SO. 1965. Specific carcinoembryonic antigens of the human digestive system. J Exp Med 122:467–481.
15. Hammarstrom S. 1999. The carcinoembryonic antigen (CEA) family: Structures, suggested functions and expression in normal and malignant tissues. Semin Cancer Biol 9:67–81.
16. Prall F, Nollau P, Neumaier M, Haubeck HD, Drzeniek Z, Helmchen U, Loning T, Wagener C. 1996. CD66a (BGP), an adhesion molecule of the carcinoembryonic antigen family, is expressed in epithelium, endothelium, and myeloid cells in a wide range of normal human tissues. J Histochem Cytochem 44:35–41.
17. Metze D, Bhardwaj R, Amann U, Eades-Perner AM, Neumaier M, Wagener C, Jantscheff P, Grunert F, Luger TA. 1996. Glycoproteins of the carcinoembryonic antigen (CEA) family are expressed in sweat and sebaceous glands of human fetal and adult skin. J Invest Dermatol 106:64–69.
18. Nap M, Hammarstrom ML, Bormer O, Hammarstrom S, Wagener C, Handt S, Schreyer M, Mach JP, Buchegger F, von Kleist S, Gruner F, Sequin P, Fuks A, Holm R, Lamerz R. 1992. Specificity and affinity of monoclonal antibodies against carcinoembryonic antigen. Cancer Res 52:2329–2339.
19. Goldenberg DM, Kim EE, DeLand FH, Bennett S, Primus FJ. 1980. Radioimmunodetection of cancer with radioactive antibodies to carcinoembryonic antigen. Cancer Res 40:2984–2992.
20. Hughes K, Pinsky CM, Petrelli NJ, Moffat FL, Patt YZ, Hammershaimb L, Goldenberg DM. 1997. Use of carcinoembryonic antigen radioimmunodetection and computed tomography for predicting the resectability of recurrent colorectal cancer. Ann Surg 226:621–631.
21. Sharkey RM, Karacay H, Griffiths GL, Behr TM, Blumenthal RD, Mattes MJ, Hansen HJ, Goldenberg DM. 1997. Development of a streptavidin-anticarcinoembryonic antigen antibody, radiolabeled biotin pretargeting method for radioimmunotherapy of colorectal cancer. Studies in a human colon cancer xenograft model. Bioconjug Chem 8:595–604.
22. Stein R, Goldenberg DM. 2004. A humanized monoclonal antibody to carcinoembryonic antigen, labetuzumab, inhibits tumor growth and sensitizes human medullary thyroid cancer xenografts to dacarbazine chemotherapy. Mol Cancer Therapeut 3:1559–1564.
23. Blumenthal RD, Osorio L, Hayes MK, Horak ID, Hansen HJ, Goldenberg DM. 2005. Carcinoembryonic antigen antibody inhibits lung metastasis and augments chemotherapy in a human colonic carcinoma xenograft. Cancer Immunol Immunother 54: 315–327.
24. Wagener C, Clark BR, Rickard KJ, Shively JE. 1983. Monoclonal antibodies for carcinoembryonic antigen and related antigens as a model system: Determination of affinities and specificities of monoclonal antibodies by using biotin-labeled antibodies and avidin as precipitating agent in a solution phase immunoassay. J Immunol 130:2302–2307.
25. Garg A, Balthasar JP. 2007. Physiologically-based pharmacokinetic (PBPK) model to predict IgG tissue kinetics in wild-type and FcRn-knockout mice. J Pharmacokinet Pharmacodyn 34:687–709.
26. Antohe F, Radulescu L, Gafencu A, Ghetie V, Simionescu M. 2001. Expression of functionally active FcRn and the differentiated bidirectional transport of IgG in human placental endothelial cells. Hum Immunol 62:93–105.
27. McCarthy KM, Lam M, Subramanian L, Shakya R, Wu Z, Newton EE, Simister NE. 2001. Effects of mutations in potential phosphorylation sites on transcytosis of FcRn. J Cell Sci 114:1591–1598.
28. Praetor A, Ellinger I, Hunziker W. 1999. Intracellular traffic of the MHC class I-like IgG Fc receptor, FcRn, expressed in epithelial MDCK cells. J Cell Sci 112:2291–2299.
29. Rojas R, Apodaca G. 2002. Immunoglobulin transport across polarized epithelial cells. Nat Rev Mol Cell Biol 3:944–955.
30. Raghavan M, Chen MY, Gastinel LN, Bjorkman PJ. 1994. Investigation of the interaction between the class I MHC-related Fc receptor and its immunoglobulin G ligand. Immunity 1:303–315.
31. Ward ES, Zhou J, Ghetie V, Ober RJ. 2003. Evidence to support the cellular mechanism involved in serum IgG homeostasis in humans. Int Immunol 15:187–195.
32. Baxter LT, Zhu H, Mackensen DG, Jain RK. 1994. Physiologically based pharmacokinetic model for specific and nonspecific monoclonal antibodies and fragments in normal tissues and human tumor xenografts in nude mice. Cancer Res 54:1517–1528.
33. Covell DG, Barbet J, Holton OD, Black CD, Parker RJ, Weinstein JN. 1986. Pharmacokinetics of monoclonal immunoglobulin G1, F(ab′)2, and Fab′ in mice. Cancer Res 46:3969–3978.
34. Flessner MF, Lofthouse J, Zakariael R. 1997. In vivo diffusion of immunoglobulin G in muscle:

Effects of binding, solute exclusion, and lymphatic removal. Am J Physiol 273:H2783–H2793.
35. Baxter LT, Zhu H, Mackensen DG, Butler WF, Jain RK. 1995. Biodistribution of monoclonal antibodies: Scale-up from mouse to human using a physiologically based pharmacokinetic model. Cancer Res 55:4611–4622.
36. Zhou J, Johnson JE, Ghetie V, Ober RJ, Ward ES. 2003. Generation of mutated variants of the human form of the MHC class I-related receptor, FcRn, with increased affinity for mouse immunoglobulin G. J Mol Biol 332:901–913.
37. Hansen RJ, Balthasar JP. 2003. Pharmacokinetic/pharmacodynamic modeling of the effects of intravenous immunoglobulin on the disposition of antiplatelet antibodies in a rat model of immune thrombocytopenia. J Pharm Sci 92:1206–1215.
38. Zhu H, Melder RJ, Baxter LT, Jain RK. 1996. Physiologically based kinetic model of effector cell biodistribution in mammals: Implications for adoptive immunotherapy. Cancer Res 56:3771–3781.
39. Chung JK, Jang JJ, Lee DS, Lee MC, Koh CS. 1994. Tumor concentration and distribution of carcinoembryonic antigen measured by in vitro quantitative autoradiography. J Nucl Med 35:1499–1505.
40. Shockley TR, Lin K, Nagy JA, Tompkins RG, Yarmush ML, Dvorak HF. 1992. Spatial distribution of tumor-specific monoclonal antibodies in human melanoma xenografts. Cancer Res 52:367–376.
41. Juweid M, Neumann R, Paik C, Perez-Bacete MJ, Sato J, van Osdol W, Weinstein JN. 1992. Micropharmacology of monoclonal antibodies in solid tumors: Direct experimental evidence for a binding site barrier. Cancer Res 52:5144–5153.
42. Hansen RJ, Balthasar JP. 2002. Intravenous immunoglobulin mediates an increase in anti-platelet antibody clearance via the FcRn receptor. Thromb Haemost 88:898–899.
43. D'Argenio DZ, Schumitzky A. 1997. ADAPT II user's guide: Pharmacokinetic/pharmacodynamic systems analysis software. Los Angeles: Biomedical Simualtion Resource.
44. Emond C, Birnbaum LS, DeVito MJ. 2006. Use of a physiologically based pharmacokinetic model for rats to study the influence of body fat mass and induction of CYP1A2 on the pharmacokinetics of TCDD. Environ Health Perspect 114:1394–1400.
45. Jensenius JC, Williams AF. 1974. The binding of anti-immunoglobulin antibodies to rat thymocytes and thoracic duct lymphocytes. Eur J Immunol 4:91–97.
46. Friedrich SW, Lin SC, Stoll BR, Baxter LT, Munn LL, Jain RK. 2002. Antibody-directed effector cell therapy of tumors: Analysis and optimization using a physiologically based pharmacokinetic model. Neoplasia 4:449–463.
47. Lammerts van Bueren JJ, Bleeker WK, Bogh HO, Houtkamp M, Schuurman J, van de Winkel JG, Parren PW. 2006. Effect of target dynamics on pharmacokinetics of a novel therapeutic antibody against the epidermal growth factor receptor: Implications for the mechanisms of action. Cancer Res 66:7630–7638.
48. Ng CM, Stefanich E, Anand BS, Fielder PJ, Vaickus L. 2006. Pharmacokinetics/pharmacodynamics of nondepleting anti-CD4 monoclonal antibody (TRX1) in healthy human volunteers. Pharm Res 23:95–103.
49. Rojas JR, Taylor RP, Cunningham MR, Rutkoski TJ, Vennarini J, Jang H, Graham MA, Geboes K, Rousselle SD, Wagner CL. 2005. Formation, distribution, and elimination of infliximab and anti-infliximab immune complexes in cynomolgus monkeys. J Pharmacol Exp Ther 313:578–585.
50. Halpern SE, Hagan PL, Garver PR, Koziol JA, Chen AW, Frincke JM, Bartholomew RM, David GS, Adams TH. 1983. Stability, characterization, and kinetics of 111In-labeled monoclonal antitumor antibodies in normal animals and nude mouse-human tumor models. Cancer Res 43:5347–5355.
51. Ferl GZ, Wu AM, DiStefano JJ III. 2005. A predictive model of therapeutic monoclonal antibody dynamics and regulation by the neonatal Fc receptor (FcRn). Ann Biomed Eng 33:1640–1652.
52. Ferl GZ, Kenanova V, Wu AM, DiStefano JJ III. 2006. A two-tiered physiologically based model for dually labeled single-chain Fv-Fc antibody fragments. Mol Cancer Therapeut 5:1550–1558.
53. Dedrick RL. 1973. Animal scale-up. J Pharmacokinet Biopharm 1:435–461.